Department Of Aerospace Engineering
Indian Institute Of Technology Madras

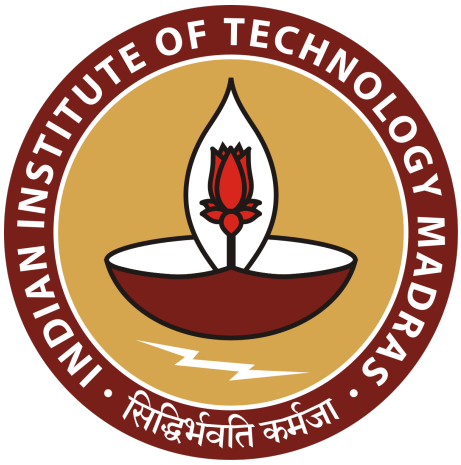

AS5470
Unsteady Aerodynamics of Moving Bodies

Project Report

Wake Capture and Load Calculation for Asymmetrically Flapping Wings

Group 9

Abhijeet Nair (*AE20B101*)

Pramat Shastri Jois (*AE20B107*)

Yogenraj Pravin Patil (*AE20B110*)

April 29, 2023

Contents

1 Introduction

This project aims to study the *wake generation* and *load generation* in an asymmetrically flapping flat plate with plunge motion. The main motivation behind this project is to understand the flapping wing motion of birds and insects which are capable of generating lift to support their own weight, and even generate thrust to fly forwards with plunging motion. The methodology followed in this project is based on Chapter 13, Section 7 of [1].

2 Framework

This section defines the framework of this study by clarifying the motion and the frame of reference used to capture the wake and generate the load.

Harmonic vs. Asymmetric Motion

In Harmonic flapping, both the upstroke and down stroke have the same frequency, so the motion is seen like a sinusoidal motion. Whereas, in Asymmetric flapping, the upstroke and down stroke have different frequencies. For this study, the asymmetric motion over a time period is modelled with half of the time period with a frequency f_1 and the remaining half to be f_2. This is implemented by first choosing a frequency f_1 and then $f_2 = nf_1$, where n is the frequency ratio. In Fig. 1, the Harmonic frequency $f_s = 1$ Hz and the Asymmetric frequency is $f_1 = f_s = 1$ Hz and $f_2 = 3$ Hz.

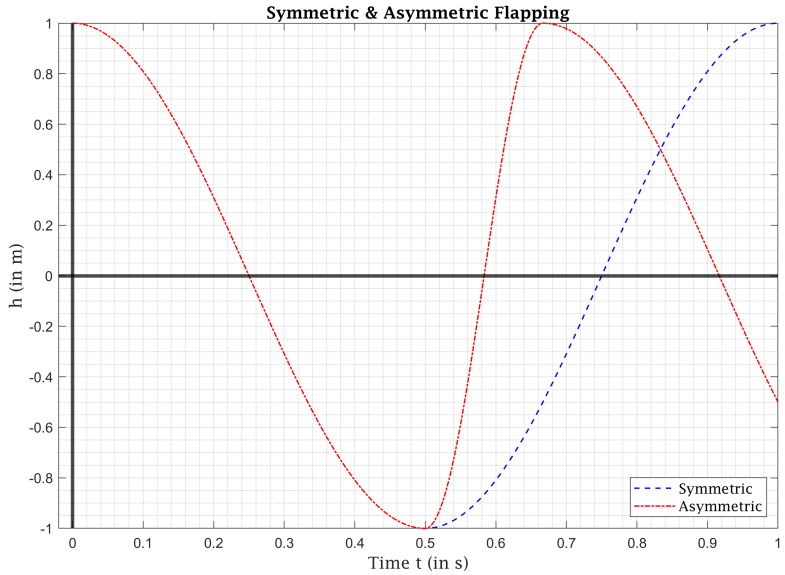

Figure 1: Harmonic vs. Asymmetric Flapping Motion

Frame of reference

The motion of the flat plate is seen from a fluid fixed frame. So, the unsteady airfoil frame of reference is defined as $(x,\ y)$ and the aerodynamic frame of reference is defined as $(X,\ Y)$. So, if the free-stream velocity, U_∞, is incident at an angle of attack α to the plunging flat plate. With this definition of frame, the motion can be visualized as the flat plate moving with free-stream velocity (U_∞) along the negative X-axis and it plunges with $\dot{h}(t)$ along the Y-axis. This can seen in Fig. 2.

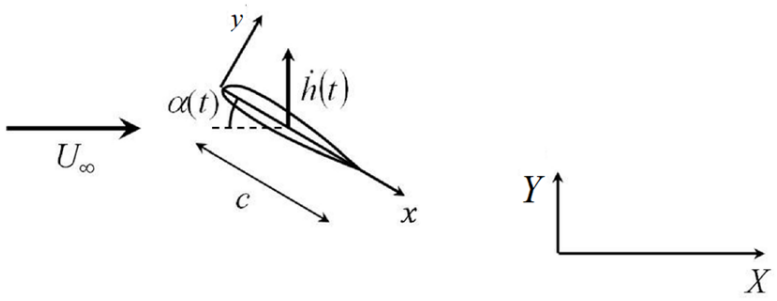

Figure 2: Fluid Frame of reference[2]

3 Algorithm

Wake Capture

Consider a flat plate in a free stream at an angle of attack α. Before the time $t = 0$, there is no circulation over the body. Let us consider only 2 elements (panels), i.e., 2 lumped vortex elements and 2 collocation points are present at the quarter and three-fourths of the element, respectively. This implies that the influence coefficient matrix is a square matrix of order 2.

Step-1: Calculate the influence coefficients using `getIndVel` function at collocation points (x_c, y_c) due to the presence of vortex element/wake element (as generated in further time steps) at (x_v, y_v). Initially, These influence coefficients are calculated by assuming vortices of unit strength, and the unknown value is then calculated later in Step-2.

Step-2: Find the unknown vortex strength and wake strength using the no-normal velocity boundary condition and Kelvin's circulation theorem.
At a time, say $t = t_1$, we have circulation $\Gamma_{b_1}(t_1)$ and $\Gamma_{b_2}(t_1)$ developing at the quarter chord of each element and the first wake with strength $\Gamma_{w_1}(t_1)$ develops simultaneously as the timer starts from zero. We fix the position of the upcoming wake at $0.1 \times (dx)$ from the trailing edge of the flat plate, where dx is the length of the element. As the wake gets generated, the influence coefficients are calculated in a similar manner and stored in a matrix B_{ij} where the indices i and j share the same nomenclature as that in step-1. The unknowns at the first time step i.e. at $t = t_1$ or $m = 1$ are $\Gamma_{b_1}(t_1)$, $\Gamma_{b_2}(t_1)$ and Γ_{w_1}. These unknowns can be calculated using no normal velocity boundary condition and the Kelvin circulation theorem. Now, as the time step increases, the new wake gets generated at the same position as the earlier one, i.e., at $0.1 \times (dx)$ from the trailing edge of the flat plate. Consider 3^{rd} time-step ($m = 3$), at which the unknows will be $\Gamma_{b_1}(t_3)$, $\Gamma_{b_2}(t_3)$ and Γ_{w_3}. From the no-normal velocity boundary condition, we have the equation

$$\begin{bmatrix} A_{11} & A_{12} \\ A_{21} & A_{22} \end{bmatrix} \begin{bmatrix} \Gamma_{b_1}(t_3) \\ \Gamma_{b_2}(t_3) \end{bmatrix} + \begin{bmatrix} B_{11} \\ B_{21} \end{bmatrix} \Gamma_{w_1} + \begin{bmatrix} B_{12} \\ B_{22} \end{bmatrix} \Gamma_{w_2} + \begin{bmatrix} B_{13} \\ B_{23} \end{bmatrix} \Gamma_{w_3} + \begin{bmatrix} u \sin\alpha - \dot{y} \cos\alpha \\ u \sin\alpha - \dot{y} \cos\alpha \end{bmatrix} = 0 \quad (1)$$

where A_{ij} and B_{ij} refer to velocity induced at collocation point i due to the presence of vortex at location j. The A and B matrices correspond to the influence coefficients due to vortex elements on the flat plate and the wakes generated respectively.

Applying Kelvin's circulation theorem at 3^{rd} time-step, we obtain the equation

$$\Gamma_{b_1}(t_3) + \Gamma_{b_2}(t_3) + \Gamma_{w_1} + \Gamma_{w_2} + \Gamma_{w_3} = 0 \quad (2)$$

Now, extending the above argument for 'N' collocation points and repacking all the equations in the matrix form, we arrive at Eqn. 3 and compute the strength of all body vortices and the strength of the wake generated at the m^{th} time step.

$$\begin{bmatrix} A_{11} & A_{12} & \dots & A_{1N} & B_{1m} \\ A_{21} & A_{22} & \dots & A_{2N} & B_{2m} \\ \vdots & \vdots & \ddots & \vdots & \vdots \\ A_{N1} & A_{N2} & \dots & A_{NN} & B_{Nm} \\ 1 & 1 & \dots & 1 & 1 \end{bmatrix} \begin{bmatrix} \Gamma_{b_1}(t_m) \\ \Gamma_{b_2}(t_m) \\ \vdots \\ \Gamma_{b_N}(t_m) \\ \Gamma_{w_m} \end{bmatrix} = \begin{bmatrix} -EF - \sum_{j=1}^{m-1} B_{1j}\Gamma_{w_j} \\ -EF - \sum_{j=1}^{m-1} B_{2j}\Gamma_{w_j} \\ \vdots \\ -EF - \sum_{j=1}^{m-1} B_{Nj}\Gamma_{w_j} \\ -\sum_{j=1}^{m-1} \Gamma_{w_j} \end{bmatrix} \tag{3}$$

where $EF = u\sin\alpha - \dot{y}\cos\alpha$ is the external flow (EF) and common to all the terms in Eqn. 1. The reason behind the summation over the term in the RHS of Eqn. 3 $B_{ij}\Gamma_{w_j}$ running from $j = 1$ to $j = m-1$ is that, at the m^{th} time step, the wake strength and the influence coefficients at the collocation points due to the wakes generated at $(m-1)^{th}$ time step are known while that of the wake generated at m^{th} time step is yet to be calculated. Also, since the new wake at every time step gets generated at a distance of $0.1 \times (dx)$ from the trailing edge of the plate, the elements B_{km} do not change at any further time step. In other words, $B_{k1} = B_{k2} = ... = B_{km}$.

Step-3: The next step is to calculate the induced velocities at the location of the latest wake generated due to all other body vortices using Eqn 4.

$$[u_w, v_w] = \texttt{getIndVel}(\Gamma, x_c, y_c, x_v, y_v) \tag{4}$$

Step-4: The position of the new wake can then be found by updating its location with that of the old position plus the distance traveled in incremental time 'dt' with a velocity (u_w, v_w) as mentioned in Eqn. 5.

$$\begin{aligned} x_w &= x_w + u_w dt \\ y_w &= y_w + v_w dt \end{aligned} \tag{5}$$

Load Generation

To compute the lift, the small disturbance approximation $(U_\infty \gg \nabla\Phi)$ is applied to the unsteady Bernoulli equation written in Eq. 6.

$$\nabla\left(\frac{\partial\Phi}{\partial t} + \frac{P}{\rho} + \frac{v^2}{2}\right) = 0 \tag{6}$$

The small disturbance approximation is used to modify the velocity term. Then performing line integration to the Eq. 6 from a reference point to the point of interest, the following expression is obtained

$$p_\infty - p = \rho\left[(U_\infty, 0, 0)\cdot\nabla\Phi + \frac{\partial\Phi}{\partial t}\right] \tag{7}$$

where, p_∞ is the pressure at some reference point, U_∞ represents the free-stream velocity and $\nabla\Phi$ is the induced velocity. Now, the pressure difference between the airfoil's upper and lower surface is computed using the Eq. 7.

$$\Delta p = 2\rho\left(U_\infty \cdot \frac{\gamma}{2} + \frac{\partial\Phi}{\partial t}\right) = \rho U_\infty \gamma(x) + \rho\frac{\partial}{\partial t}\int_0^x \gamma(x)dx \tag{8}$$

Here, for a planar vortex distribution on a flat plate, the jump in velocity is $\frac{\gamma}{2}$. So, the upper surface induced velocity is taken as $\nabla\Phi = (\gamma/2, 0, 0)$. with this consideration, Φ can be written as $\Phi = \int_0^x \gamma(x)dx$.

For the lumped-vortex method, there is only one airfoil vortex and therefore the lift L' per unit span is calculated as

$$L' = \int_0^c \Delta p dx \tag{9}$$

For the N number of lumped vortices on the body, the lift equation can be given as

$$L'(t_m) = \rho \left[U_\infty \sum_{i=1}^{N} \Gamma_{b_i}(t_m) + c\frac{\partial}{\partial t}\left(\sum_{i=1}^{N} \Gamma_{b_i}(t_m) \right) \right] \tag{10}$$

The lift equation has two terms. The first is due to the wake-induced downwash, which rotates the circulatory lift term by an induced angle v_w/U_∞. The second is due to the fluid acceleration $\partial\Phi/\partial t$ which acts normal to the flat plate and its contribution to the drag is α times the second lift term in Eq. 11. Next, the drag force per unit span for N lumped vortices is

$$D(t_m) = \rho \left[\sum_{i=1}^{N} v_w(x_i, t_m)\Gamma_{b_i}(t_m) + c\alpha\frac{\partial}{\partial t}\left(\sum_{i=1}^{N} \Gamma_{b_i}(t_m) \right) \right] \tag{11}$$

Here again, the first term is due to the wake-induced downwash $v_W(x,t)$, which in the lumped vortex case is evaluated at the three-quarter chord point or collocation point. The second term is due to the fluid acceleration.

4 Results & Discussion

1) Symmetric Flapping:

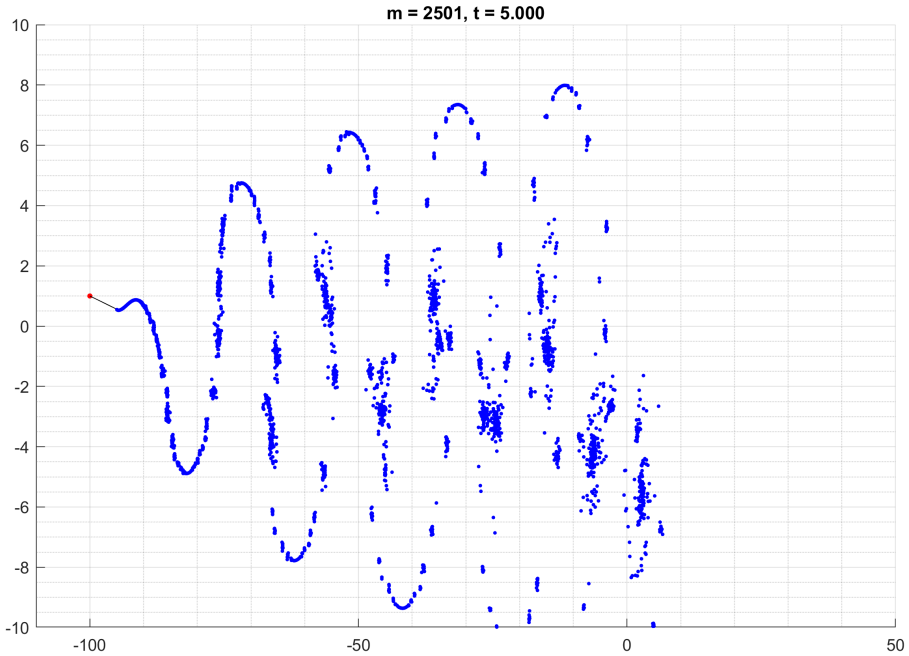

Figure 3: Wake structure

First, we check the case of symmetric flapping. Here, the upstroke and downstroke have the same frequency of $f_1 = f_2 = 1$ Hz. The amplitude of the strokes is kept as 1 m. Also, we have the freestream velocity as 20 m/s, angle of attack $\alpha = 5°$. We have considered 10 panels on th body. The wake structure is given in Fig. 3. The loads and its coefficients are given in Figs. 4 & 5.

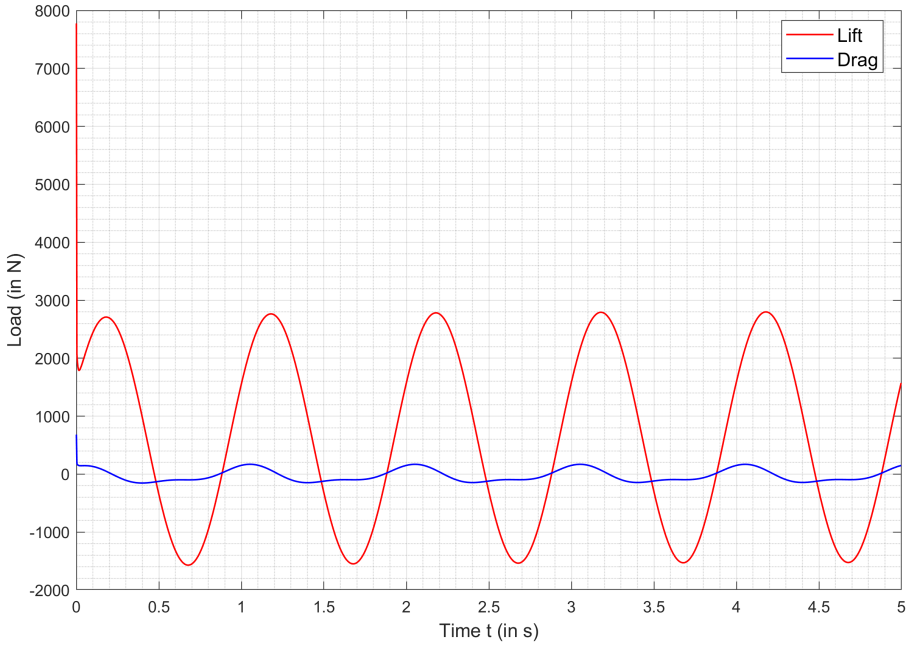

Figure 4: Loads generated

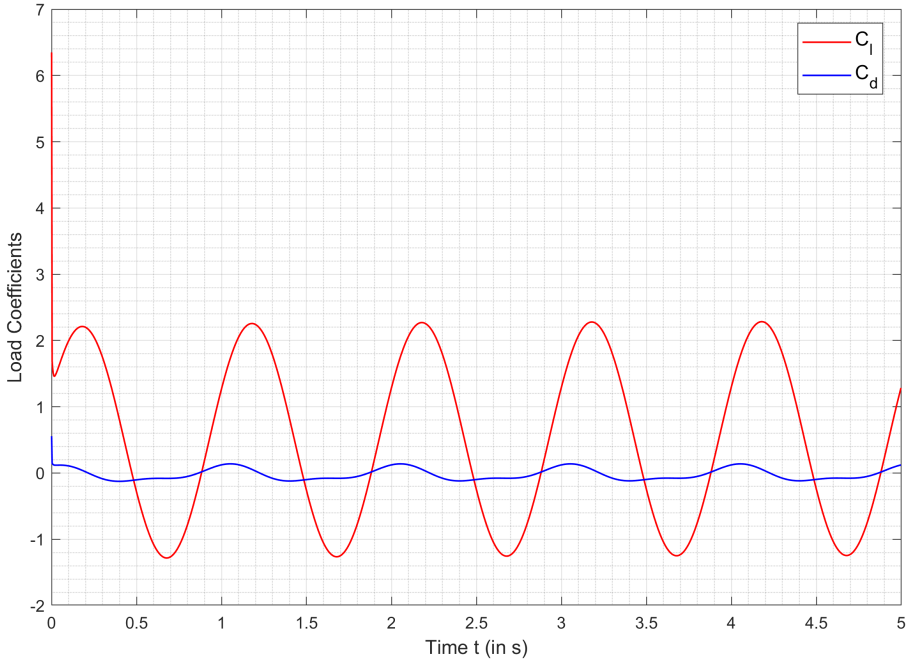

Figure 5: Coefficient of loads generated

Here, we observe that a *Reverse Karman* wake structure. Also, the mean lift coefficient $C_l = 0.5137$ and mean drag coefficient $C_d = -0.0198$. This indicates that there is a net thrust on the body. This also proves the fact that **the Reverse Karman is a thrust producing wake**.

2) Asymmetric flapping ($n = 4$, $f_1 = 1$ Hz, $f_2 = 4$ Hz):

In this case, we have the downstroke frequency as 1 Hz and upstroke frequency as 4 Hz. Rest of the flow parameters remain same. Fig. 6 shows the wake structure and Figs. 7 & 8 show the loads generated and it's coefficients.

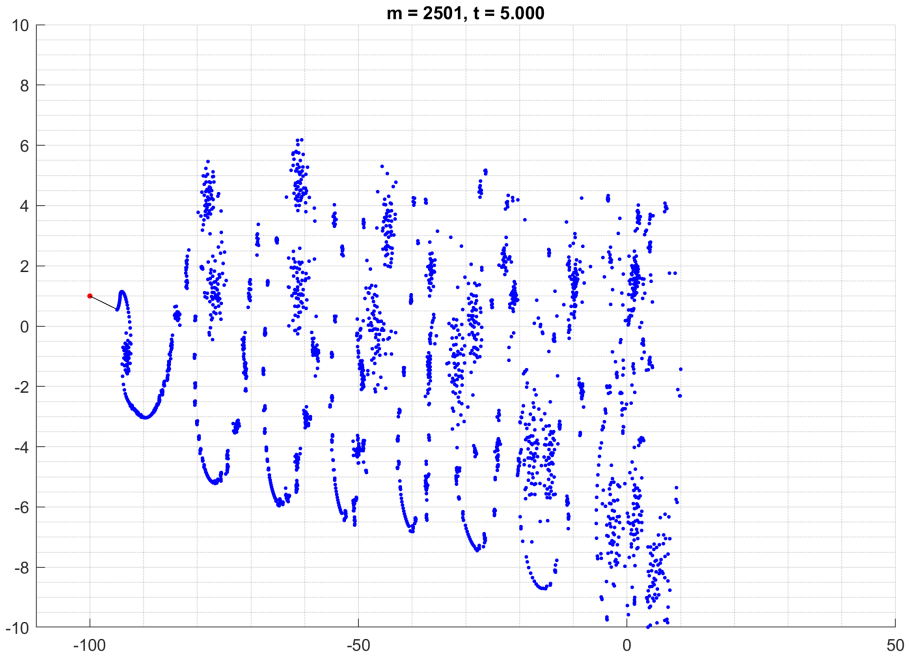

Figure 6: Wake structure

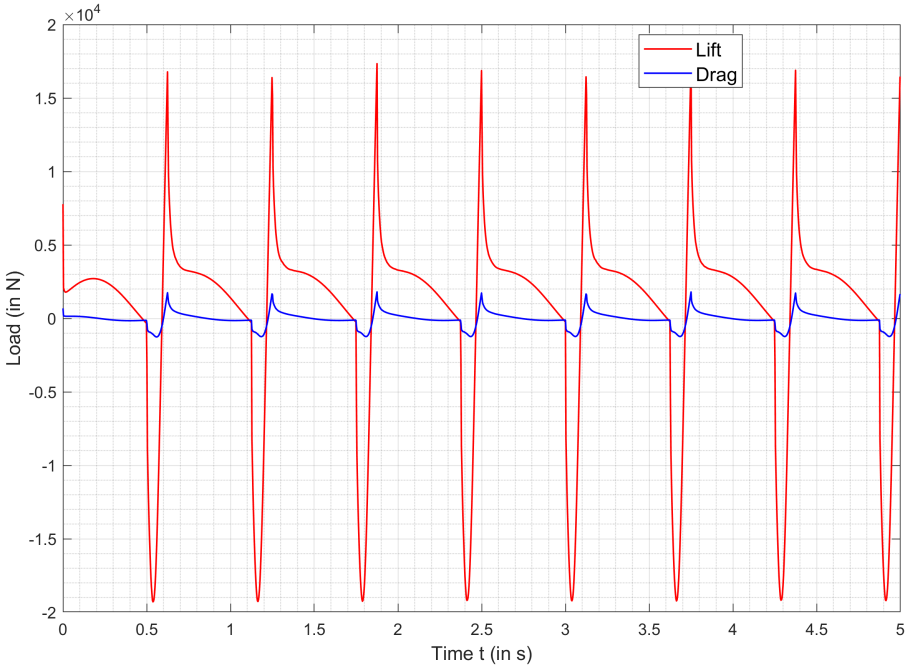

Figure 7: Loads generated

Here, we again observe a *Reverse Karman* wake structure. The mean load coefficients are $C_l = 0.4883$ & $C_d = -0.0461$. Thus, we again observe a thrusting effect on the body. We also observed the wake structures generated during the sudden upstroke to be eventually following a deflected path, suggesting a *deflected Reverse Karman* structure. Also, we can

observe that the symmetry in the wake has been lost. We also see certain small sub-structures forming between the bigger structures.

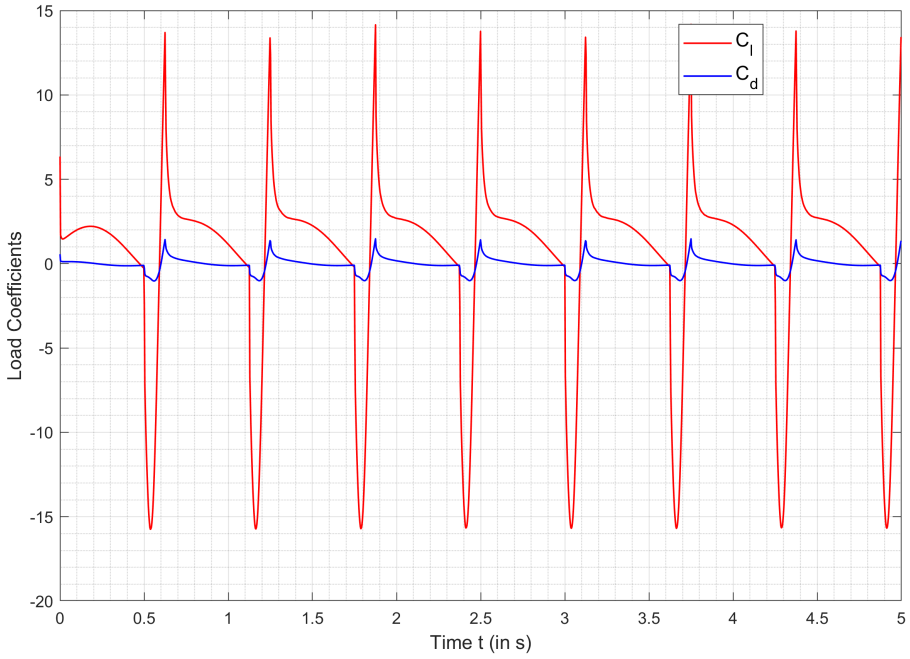

Figure 8: Coefficient of loads generated

3) Asymmetric flapping ($n = 8$, $f_1 = 1$ Hz, $f_2 = 8$ Hz):

In this case, we have the downstroke frequency as 1 Hz and upstroke frequency as 8 Hz. Rest of the flow parameters remain same. Fig. 9 shows the wake structure and Figs. 10 & 11 show the loads generated and it's coefficients.

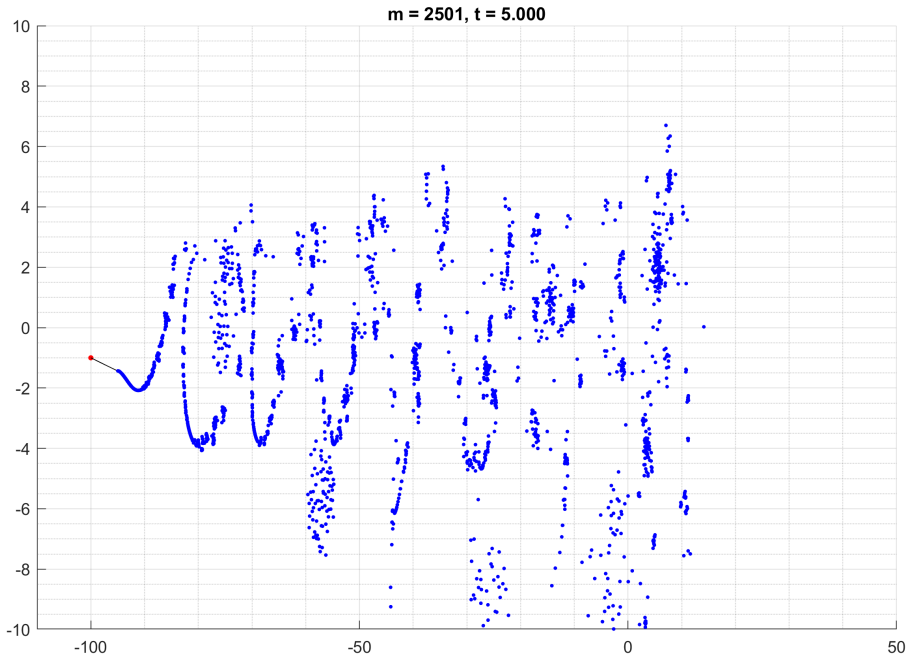

Figure 9: Wake structure

A similar observation as above (Case-2) is made here as well. The mean load coefficients are $C_l = 0.5884$ & $C_d = -0.1059$. The primary differences are the increase in the intensity of movement of the wakes. Also, we can see over the past three cases, that the C_l & C_d (both

mean and maximum) have been steadily increasing. This suggests that flapping faster gives a higher load carrying capacity.

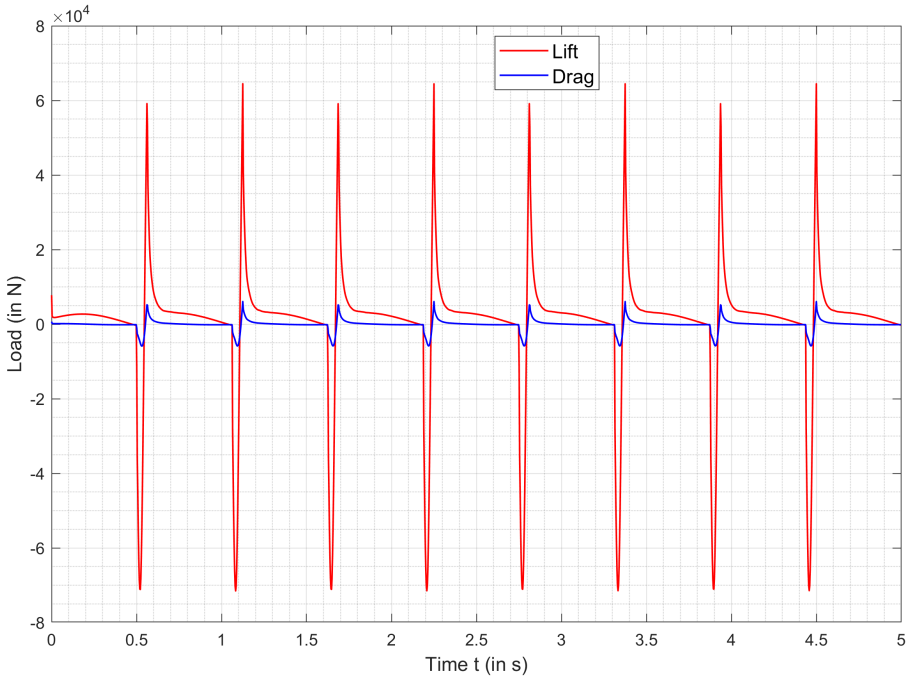

Figure 10: Loads generated

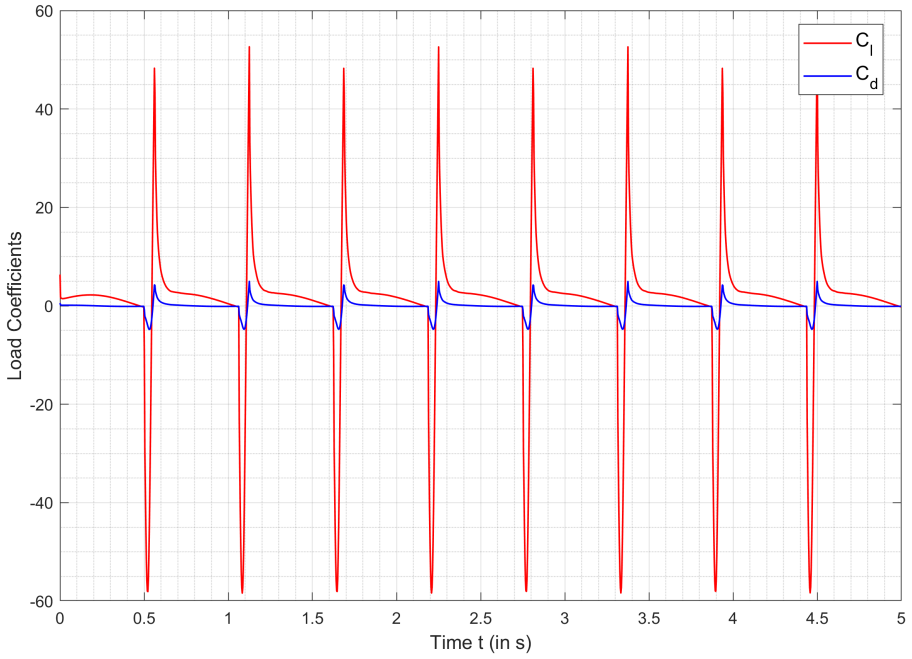

Figure 11: Coefficient of loads generated

4) Asymmetric flapping ($n = 1/4$, $f_1 = 4$ Hz, $f_2 = 1$ Hz):

In this case, we have the downstroke frequency as 4 Hz and upstroke frequency as 1 Hz. Rest of the flow parameters remain same. Fig. 12 shows the wake structure and Figs. 13 & 14 show the loads generated and it's coefficients.

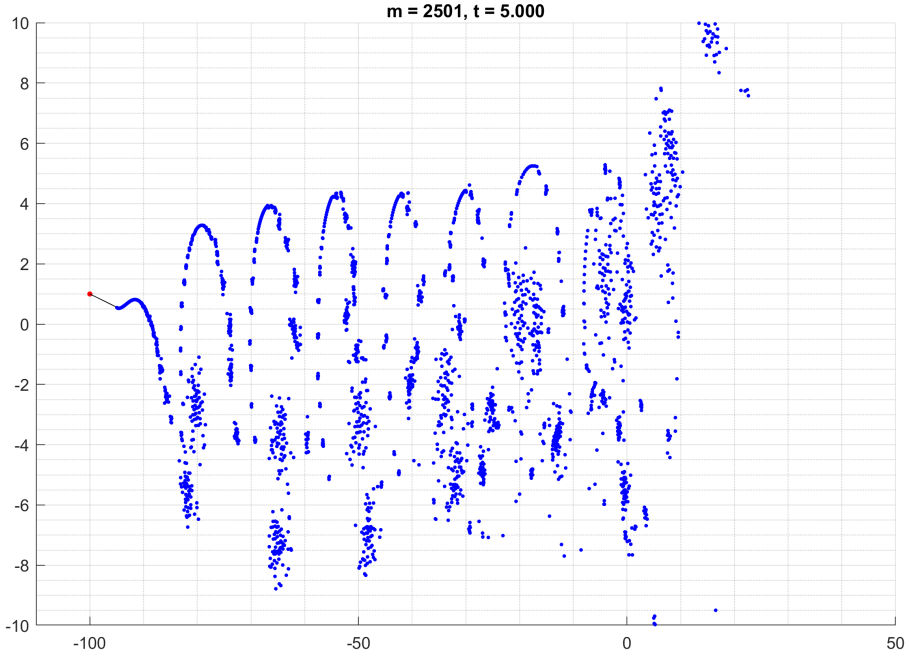

Figure 12: Wake structure

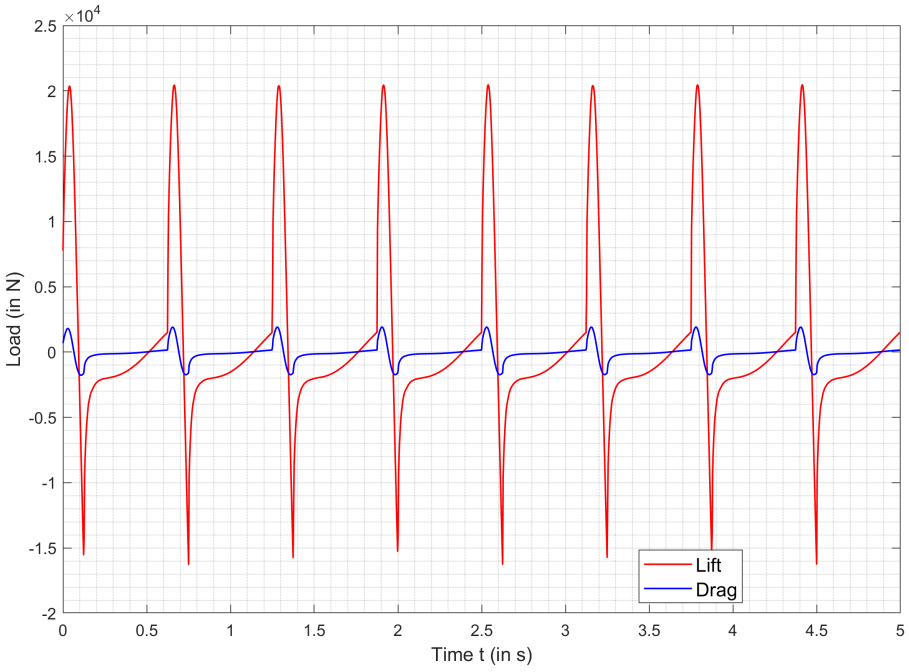

Figure 13: Loads generated

Here, we basically have a mirror image as in Case-2. All the properties are similar. The mean load coefficients are $C_l = 0.4870$ & $C_d = -0.0534$.

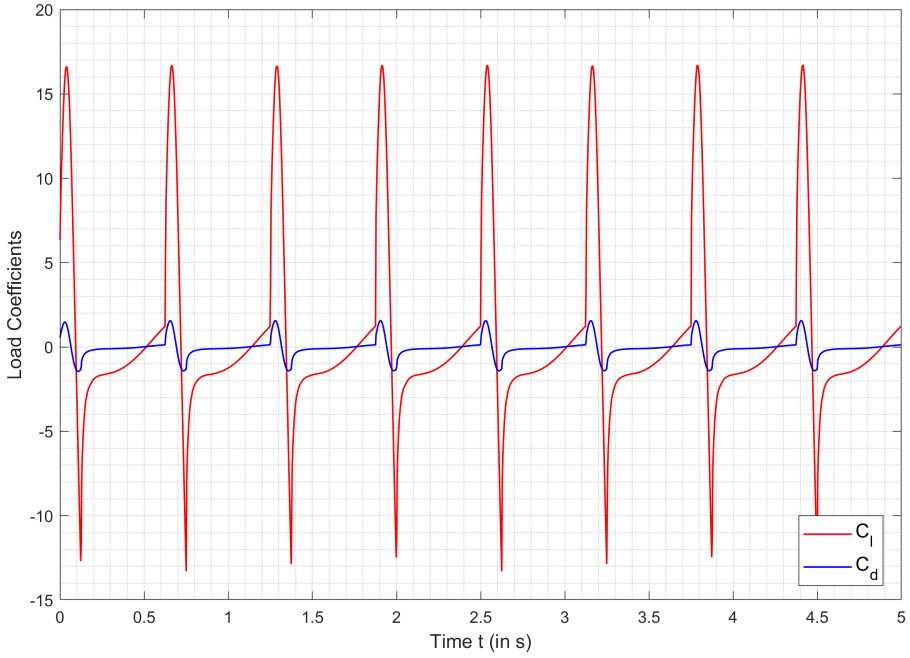

Figure 14: Coefficient of loads generated

Tab. 1 summarises the values of load coefficients C_l and C_d for the four cases above. We observe a increase in the coefficients as we increase flapping frequency, as we had mentioned earlier.

Case	C_l	C_d
Symmetric	0.5137	-0.0198
Asymmetric ($n = 4$)	0.4883	-0.0461
Asymmetric ($n = 8$)	0.5884	-0.1059
Asymmetric ($n = 1/4$)	0.4870	-0.0534

Table 1: Load coefficients

5 Conclusions

From this study, the interesting observation and a few concluding remarks from these observations is summarised as follows.

1. **Reverse Karman** wake structure was observed in all cases.
2. All cases were observed to have a negative mean drag coefficient, which indicated a net thrusting effect on the body.
3. From the previous observation, it can be inferred that the **Reverse Karman** wake is a thrusting wake, i.e., it produces a net thrust on the body.
4. It was also observed that the lift and coefficient of lift increase as the frequency of the flapping was increased (Tab. 1). Same observation is also true for the drag and drag coefficient.

References

[1] J. Katz and A. Plotkin, *Low-Speed Aerodynamics*. Cambridge Aerospace Series, Cambridge University Press, 2001.

[2] T. Faure, L. Dumas, and O. Montagnier, "Numerical study of two-airfoil arrangements by a discrete vortex method," *Theoretical and Computational Fluid Dynamics*, vol. 34, 04 2020.